Electronic Supplementary Material (ESI) for Lab on a Chip

Supplementary Information:
Large scale arrays of tunable microlenses

Atul Varshney,*[a] Smita Gohil,[a] Somayeh Khajehpour Tadavani,[b]
Anand Yethiraj,[b] S. Bhattacharya,[a] and Shankar Ghosh[a]

[a] *Department of Condensed Matter Physics and Materials Science,*
Tata Institute of Fundamental Research,
Homi Bhabha Road, Mumbai 400-005, India

[b] *Department of Physics and Physical Oceanography, Memorial University,*
St. John's, Newfoundland and Labrador, Canada, A1B 3X7

Frequency and field dependent shape deformation

The shape evolution of a single silicone oil droplet as a function of frequency is shown in Fig. S1(a). With increasing frequency, the shape of the droplet changes from an oblate spheroid to a spherical to a prolate spheroid. The equations (1, 2) are qualitatively consistent with the frequency-driven oblate to prolate transition shown in Fig. S1(a). The axes of an ellipsoid, i.e., $d_{\parallel}$ and $d_{\perp}$ are plotted against frequency in Fig. S1(b). At frequencies below $\nu_c \sim 200\ Hz$, $d_{\perp} > d_{\parallel}$; oblate spheroid, at $\nu = \nu_c$, $d_{\perp} = d_{\parallel}$; spherical droplet, and at $\nu > \nu_c$, $d_{\perp} < d_{\parallel}$; prolate spheroid. The scaled shape deformation (D/a) with frequency is shown in the inset of Fig. S1(b) which shows the shape transition at $\nu \sim 200Hz$. At frequencies 20 Hz and 1 kHz where the drop shapes are oblate and prolate respectively, we varied the amplitude of the electric field. Figure S1(c) shows the variation of (D/a) as a function of electric field intensity (E^2) for different droplet diameters shown by different colored circles. The oblate drop (at low frequency) shows a very strong dependency on E^2, however, the prolate drop displays a weak effect on E^2. This can be understood that the magnitude of the total electric stress (sum of normal and tangential stresses, and both goes as E^2) is large at low frequencies, dominated by the tangential stresses, therefore the oblate drops show strong dependency on E^2. However, at high frequencies the total stress is small (the tangential component vanishes), therefore, the deformation of the prolate drop would be less with increasing E^2 as compared to the oblate drop [1]. In order to get the large dynamic range of shapes, from oblate spheroid to spherical to prolate spheroid, we tuned

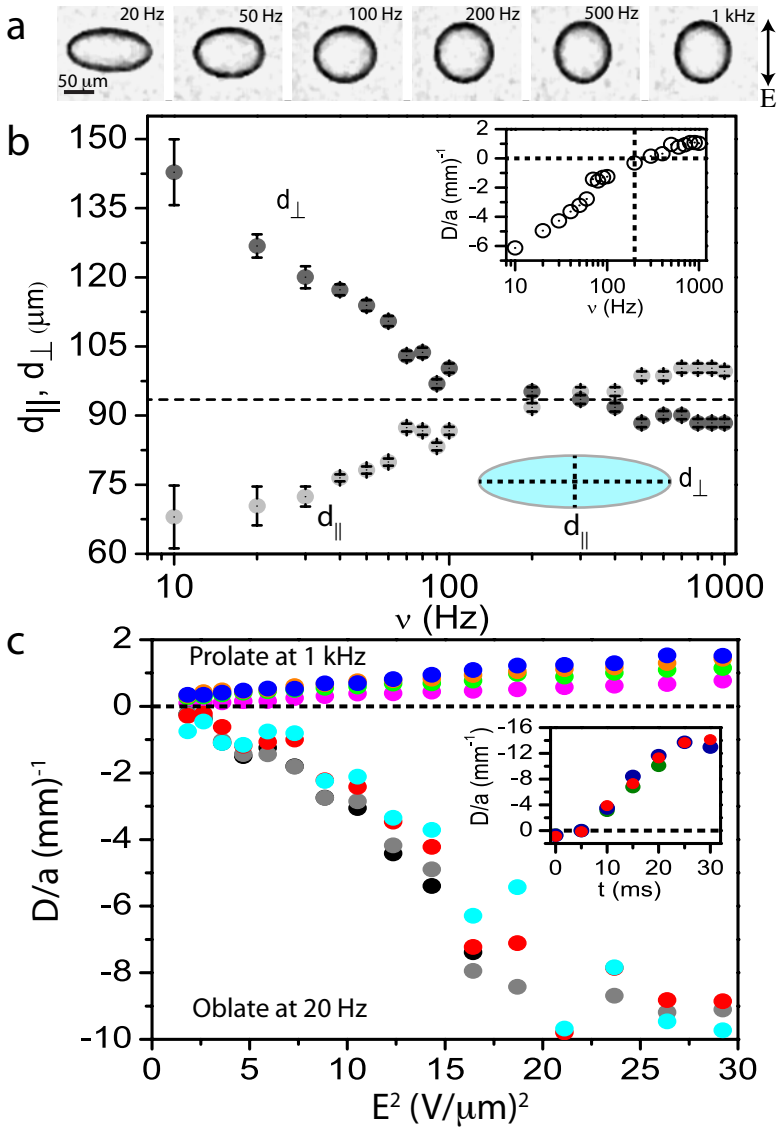

Fig. S1: (a) Shape evolution of a droplet from oblate to prolate spheroid with increasing frequency. The electric field is in the plane of the page and pointing vertically upwards. (b) Variation of minor and major axes, i.e., $d_{\parallel}$ (parallel to the field direction) and $d_{\perp}$ (perpendicular to the field direction) respectively, of an ellipsoid as a function of frequency (ν). The inset of (b) shows the plot of scaled deformation (D/a) with ν and exhibits the shape transition at $\nu_c \sim 200\ Hz$. The electric field amplitude (E) is kept constant at 5 $V/\mu m$ in (a, b). (c) The variation of (D/a), for different sized drops shown by different colored circles, as a function of electric field intensity (E^2) at $\nu = 20\ Hz$ and 1 kHz where the droplet shapes are oblate and prolate, respectively. The inset of (c) shows the time response of (D/a). The droplets at $t = 0$ are prolate (at 1 kHz) and transformed to oblate (at 10 Hz) within a span of 30 ms.

the frequency (ν) of the applied field keeping the amplitude constant at $E = 10\ V/\mu m$. We can thus synchronously change the radius of curvature, i.e., the focal length (f), of each droplet in the array (see Fig. 2) by changing the frequency. The time response of the shape deformation from a prolate, obtained at 1 kHz, to an oblate, obtained at 10 Hz, is shown in the inset of Fig. S1(c). The response time of the system for the whole dynamic range of deformation is about 30 ms which is better than reported in other systems [2–4].

Quasi-3D arrangement of droplet array

We investigated the quasi-3D droplet arrangement in the planes as a function of separation between the planes by varying the electrode spacing (but keeping the field amplitude fixed at 10 $V/\mu m$). We then repeated the same frequency cycling described above to obtain the droplet array. Figure S2(a−b) show the droplet arrangement for electrode spacing (d) of about 120 μm and 400 μm respectively, where the droplets (marked by cyan colored circles) near the bottom plane is overlaid on the droplets (marked by pink colored circles) near the top plane. Their respective drop size distribution is shown in the insets of Fig. S2(a−b). The corresponding $f-$number ($= f/2a$) distribution of droplet array (Fig. S2(a−b)) is displayed in Fig. S2(c).

The angle (ϕ) between the adjacent pairs of droplets in two planes is calculated by joining them with a vector $\vec{s}$ whose horizontal and vertical components are respectively s_x and s_y, and $\phi = tan^{-1}(s_y/s_x)$. The probability distribution of angles, $P(\phi)$, is narrow for 120 μm electrode spacing signifying the correlation of droplets positions' in the two planes, shown in Fig. S2(d). The system loses its correlation as the electrode spacing is increased to 400 μm, reflected in the broad distribution of $P(\phi)$ and shown in Fig. S2(d).

In order to understand the orientational ordering between the droplets in an array, we compute the 2D orientational bond order parameter Ψ_6 defined as [5, 6]:

$$\Psi_6(r_p) = \sum_{q=1}^{N} e^{i6\theta_{pq}}/N$$

Here, N denotes the number of nearest neighbors q of the p^{th} particle, and θ_{pq} is the bond angle between p and q particles with a fixed yet arbitrary reference axis. For a perfect 2d crystal, Ψ_6 has a value unity. The loss of crystallinity is reflected in the spatial correlation

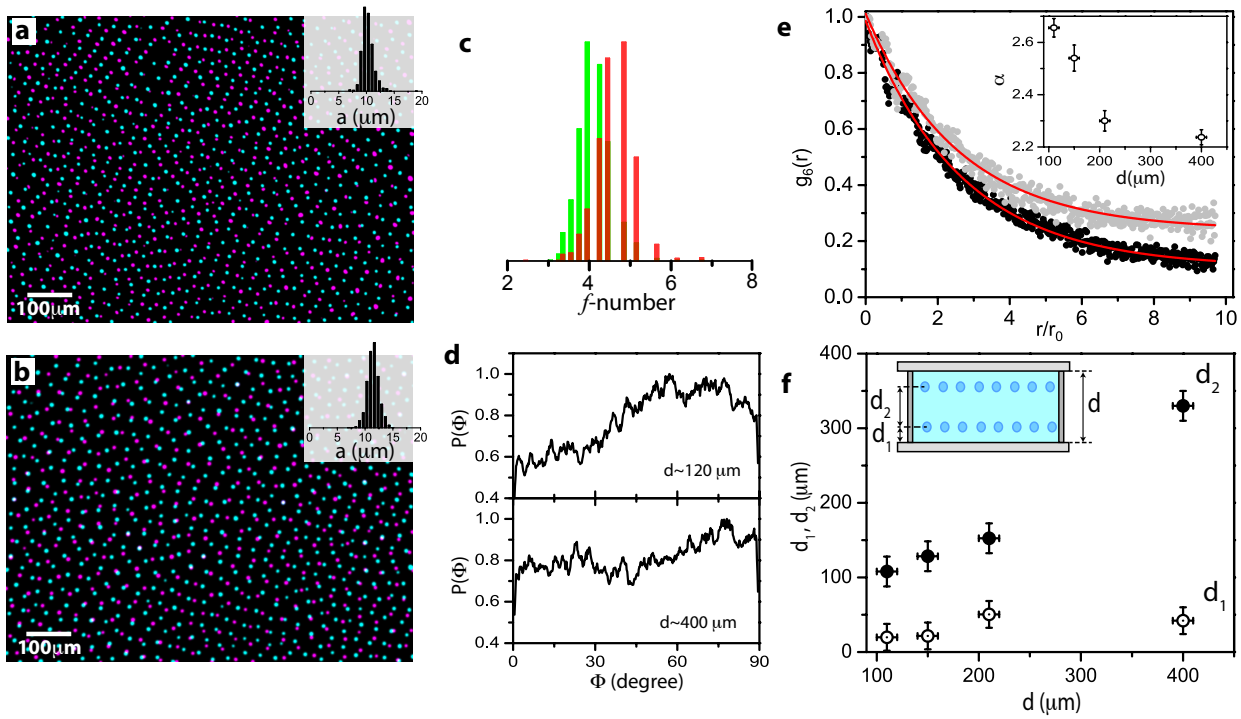

Fig. S2: Micrographs shown in (a, b) are obtained by overlaying the droplet array of two planes for electrode spacing (d) of about 120 μm and 400 μm, respectively. Insets of (a, b) show the distribution of drop radius. (c) Distribution of $f-$numbers of droplet array for $d \sim 120$ μm (red) and 400 μm (green). (d) The corresponding probability distribution of angles, $P(\phi)$, between the adjacent pairs of droplets in two planes. (e) Variation of the bond order correlation function $g_6(r)$ versus r/r_0 (where r_0 is the position of the first peak of the pair correlation function $g(r)$) for $d \sim 120$ μm (black circles) and 400 μm (gray circles). It is computed for the droplets arranged in the top plane. Red lines are exponential fits, function $Ae^{-(r/r_0)/\alpha}$, to the data. Inset shows the variation of α with d. (f) Variation of distance between the electrode surface and the adjacent droplet plane (d_1, open circles) and the separation between the two droplet planes (d_2, filled circles). Droplet arrangement is illustrated in the inset.

of the bond order parameter $g_6(r)$, given by [6]

$$g_6(r = |r_p - r_q|) =< \Psi_6^*(r_p)\Psi_6(r_q) >$$

Figure S2(e) shows the spatial variation of $g_6(r)$ for $d \sim 120$ μm and 400 μm electrode spacings for the droplets at the top plane. With increasing electrode spacing, the in-plane

correlation among the droplets becomes stronger, however, at the same instance the correlation between the droplets in two planes becomes poorer (shown in Fig. S2(d)). This is reflected in the variation of α, obtained by fitting $g_6(r)$ with an exponential function $Ae^{-\frac{r/r_0}{\alpha}}$, with d (inset of Fig. S2(e)). The separation between the two droplet planes (d_2) increases with the electrode spacing (d), shown in Fig. S2(f). However, the distance between the electrode surface and the adjacent droplet plane (d_1) does not change significantly with d (see Fig. S2(f)).

Supplementary Movie 1: In-plane localization via DEP

This movie shows that upon switching frequency from 3 Hz to 8 Hz at $E = 10\ V/\mu m$, roughly monodisperse droplets are obtained from polydisperse distribution. The movie is recorded at 2.4 fps and displayed at 7 fps.

References

[1] S. Torza, R. G. Cox and S. G. Mason, *Phil. Trans. R. Soc. Lond. A*, 1971, **269**, 295–319

[2] P. Fei, Z. He, C. Zheng, T. Chen, Y. Men and Y. Huang, *Lab Chip*, 2011, **11**, 2835–2841

[3] L. Dong, A. K. Agarwal, D. J. Beebe and H. Jiang, *Nature*, 2006, **442**, 551–554

[4] S. Yang, T. Krupenkin, P. Mach and E. Chandross, *Advanced Materials*, 2003, **15**, 940–943

[5] P. J. Steinhardt, D. R. Nelson and M. Ronchetti, *Phys. Rev. B*, 1983, **28**, 784–805

[6] X. Qi, Y. Chen, Y. Jin and Y.-H. Yang, *Journal of the Korean Physical Society*, 2006, **49**, 1682–1686